Journal of Power Sources 225 (2013) 124–128

Contents lists available at SciVerse ScienceDirect

Journal of Power Sources

journal homepage: www.elsevier.com/locate/jpowsour

Short communication

The electrochemical behaviors of Mg–8Li–3Al–0.5Zn and Mg–8Li–3Al–1.0Zn in sodium chloride solution

Yanzhuo Lv [a,*], Min Liu [a], Yan Xu [b], Dianxue Cao [a], Jing Feng [a]

[a] College of Material Science and Chemical Engineering, Harbin Engineering University, Harbin 150001, PR China
[b] College of Mechanical and Electrical, Harbin Engineering University, Harbin 150001, PR China

HIGHLIGHTS

- Zn contents would affect the performance of alloy anode of Mg–H_2O_2 semi fuel cells.
- The performance of Mg–8Li–3Al–0.5Zn is better than that of Mg–8Li–3Al–1.0Zn.
- Mg–8Li–3Al–0.5Zn alloy is suitable to use as anode of Mg–H_2O_2 semi fuel cells.

ARTICLE INFO

Article history:
Received 16 June 2012
Received in revised form
22 September 2012
Accepted 24 September 2012
Available online 29 September 2012

Keywords:
Magnesium–lithium-based alloys
Anode material
Electrochemical performance
Corrosion resistant
Magnesium–hydrogen peroxide semi fuel cells

ABSTRACT

The electrochemical oxidation behaviors of Mg–8Li–3Al–0.5Zn and Mg–8Li–3Al–1.0Zn electrodes in 0.7 mol L^{-1} NaCl solution are investigated by methods of potentiodynamic polarization, potentiostatic oxidation, electrochemical impedance spectroscopy and scanning electron microscopy. The phase composition of Mg–8Li–3Al–0.5Zn and Mg–8Li–3Al–1.0Zn alloys is analyzed conducted by X-ray diffraction. The performances of Mg–8Li–3Al–0.5Zn and Mg–8Li–3Al–1.0Zn as the anode of Mg–H_2O_2 semi fuel cells are determined. The effect of Zn content on the corrosion resistant of these Mg–Li-based alloys is studied. It is found that the Mg–8Li–3Al–0.5Zn electrode has higher discharge activity and less corrosion resistance than that of Mg–8Li–3Al–1.0Zn electrode in 0.7 mol L^{-1} NaCl solution. The Mg–H_2O_2 semi fuel cell with Mg–8Li–3Al–0.5Zn anode presents a maximum power density of 100 mW cm^{-2} at room temperature, which is higher than that of Mg–8Li–3Al–1.0Zn anode (80 mW cm^{-2}). The performance of semi fuel cell with the Mg–8Li–3Al–0.5Zn electrode is better than that with Mg–8Li–3Al–1.0Zn electrode, especially at higher current density (>30 mA cm^{-2}).

1. Introduction

Because of its high specific energy, short mechanically recharge time, long dry storage life, stable discharging ability, workability at ambient pressure, environment acceptability, safety and low cost [1–15], Mg–H_2O_2 semi fuel cell has been developed as the power source for low rate, long endurance autonomous underwater vehicle (AUV) in Naval Undersea Warfare Center and University of Massachusetts [1–9]. In order to achieve a good performance, the anode material of the Mg–H_2O_2 semi fuel cell should have the following properties: (i) high discharge activity, (ii) strong corrosion-resistance to seawater and acid, (iii) a porous structure [15].

Li has a high discharge activity and high energy density, so it can increase the discharge activity, reduce the lagging effect and improve the specific energy of Mg alloy electrodes. Mg–Li alloy with more than 5.7% Li has improved ductility than pure Mg, thus it can be easily fabricated to different shapes. Therefore, recently, Mg–Li alloys have been studied as the anode material of Mg–H_2O_2 semi fuel cell [17–20]. It has been reported that Mg–Li alloys have higher electrochemical activity than pure Mg and the commercial AZ31 alloy in 0.7 mol L^{-1} NaCl solution [18]. However, Mg–Li alloys as the anode materials also show some disadvantages, such as less corrosion resistive than pure Mg, which may be attributed to the high activity of Li. Song et al. [10] reported that a layer of hydroxyl or oxide protective coating could be formed on Mg–Li alloy surface in the air or neutral environment. It is usually loose and uneven, which can not provide a good protective effect on Mg–Li alloy. In order to enhance the performance of Mg–Li-based alloy anodes, some alloying elements were added to Mg–Li alloy, such as Al, Si, Cu, Zn. Ma et al. [16] investigated the corrosion behavior and

* Corresponding author. Tel.: +86 13845079693.
E-mail address: lvyanzhuo@hrbeu.edu.cn (Y. Lv).

0378-7753/$ – see front matter © 2012 Elsevier B.V. All rights reserved.
http://dx.doi.org/10.1016/j.jpowsour.2012.09.088

discharge performance of Mg, AZ31 and Mg–Li–Al–Ce in 3.5 wt. % NaCl solution. It was found that Mg–Li–Al–Ce has higher electrochemical activity and lower self-corrosion rate than that of Mg and AZ31. At a current density of 2.5 mA cm^{-2}, the operate voltage of the Mg–Li–Al–Ce anode is 1.272 V, the specific discharge capacity is 2076 mAh g^{-1}, and the anodic utilization efficiency is 85.2%. Cao et al. [17–19] reported that Mg–Li-based alloys, such as Mg–Li, Mg–Li–Al, Mg–Li–Al–Ce, Mg–Li–Al–Sn, Mg–Li–Al–Ce–Sn, Mg–Li–Al–Ce–Zn, and Mg–Li–Al–Ce–Zn–Mn, exhibited high electrooxidation activity in 0.7 mol L^{-1} NaCl solution. They found that Ce can enhance both the discharge activity and utilization efficiency. Sn mainly improves the discharge current. Our group recently reported the electrochemical behavior of Mg–Li–Al–Ce and Mg–Li–Al–Ce–Y alloys in 0.7 mol L^{-1} NaCl solution. It was found that Mg–Li–Al–Ce–Y alloy is more corrosion resistive than that of Mg–Li–Al–Ce. Y can change the alloy structure or assist the formation of an easy-peel off layer on the alloys surface [20].

In this study, the effects of Zn content on the electrochemical oxidation performance of Mg–Li–Al–Zn alloy were investigated. The performances of Mg–H_2O_2 semi fuel cells using the Mg–Li–Al–Zn anodes were also examined.

2. Experimental

2.1. Preparation of Mg–Li-based alloys

Mg–8Li–3Al–0.5Zn and Mg–8Li–3Al–1.0Zn alloys were prepared by vacuum melting method using high purity (>99.9%) metal ingots as the raw materials. These ingots were put into an induction furnace under the protection of ultrahigh purity argon. The furnace was then evacuated to 1.0×10^{-2} Pa, and charged with ultrahigh purity argon. AC power was applied to melt the metal raw materials under flowing argon atmosphere. The molten metals were then poured into the awaiting stainless steel mold. The mold containing hot melts was cooled down to ambient temperature under argon atmosphere in the furnace within 2 h. The nominal compositions of the alloys are given in Table 1.

2.2. Electrochemical measurements

In the electrochemical measurements, the saturated calomel electrode (SCE) was used as the reference electrode and all the potentials were quoted with respect to SCE. The platinum foil and Mg–Li-based alloys were used as the counter electrode and the working electrode, respectively. The Mg–Li-based alloy ingots were machined to 20 mm × 20 mm × 2 mm. Prior to use, the working electrode was successively polished with 120#, 360# and 600# metallographic emery papers, washed with deoxygenated ultrapure water (Milli-Q), degreased with acetone and rinsed with deoxygenated ultrapure water again, and then immediately assembled into the electrochemical cell.

A specifically designed home-made three-electrode electrochemical cell [18] was used to carry out the electrochemical measurements of Mg–Li-based alloys. The exposure area of the metal alloy electrode is 0.95 cm^2, which was used to calculate the current density. Electrochemical experiments were carried out at room temperature in 0.7 mol L^{-1} NaCl aqueous solution. It was purged with N_2 gas for 15 min before measurements in order to remove the O_2 gas dissolved in the solution.

Potentiodynamic polarization curves were obtained by sweeping the potential from −2.2 V to −0.4 V at a scan rate of 10 mV s^{-1}. Potentiostatic current–time curves were measured by holding the working electrode (alloy specimen) for 5 min at −1.0 V. Electrochemical impedance spectra were recorded under open circuit potential with the frequency range from 100 mHz to 100,000 Hz with the amplitude of 8 mV. The morphology of the alloy surface was examined using scanning electron microscopy (SEM, S4800, JSM-6480) equipped with energy dispersive spectroscopy (EDS unit). The phase structure was analyzed by X-ray diffraction (XRD, Rigaku-Dmax 2500) using Cu Kα radiation operated at 40 kV and 150 mA.

2.3. Mg–H_2O_2 semi fuel cell tests

The performance of Mg–Li-based alloys as anode of Mg–H_2O_2 semi fuel cell was examined using a home-made flow through test cell made of Plexiglas. The geometrical area of the Mg–Li-based alloys anode and the Ir/Pd coated nickel foam cathode was 4.0 cm^2 (20 mm × 20 mm). Nafion-115 membrane was used to separate the anode and the cathode compartments. The anolyte (0.7 mol L^{-1} NaCl) and the catholyte (0.7 mol L^{-1} NaCl + 0.1 mol L^{-1} H_2SO_4 + 0.5 mol L^{-1} H_2O_2) were pumped into the bottom of the anode and the cathode compartments, respectively, and exited at the top of the compartments. The flow rate for the anolyte and the catholyte was 85 mL min^{-1} and it is controlled by individual peristaltic pump.

3. Results and discussion

3.1. Phase structure

The phase composition of Mg–8Li–3Al–0.5Zn and Mg–8Li–3Al–1.0Zn alloys is analyzed by XRD and the results are shown in Fig. 1. It indicates that the alloys mainly consists of α(Mg), β(Li), Zn and Al_2Mg phases. The peak position of Mg and Li in the Mg–8Li–3Al–0.5Zn alloy is slightly different from that in the Mg–8Li–3Al–1.0Zn alloy, which may be attributed to the different lattice

Table 1
Chemical compositions of alloys (wt.%).

Alloys	Mg	Li	Al	Zn
Mg–8Li–3Al–0.5Zn	88.5	8	3	0.5
Mg–8Li–3Al–1.0Zn	88	8	3	1

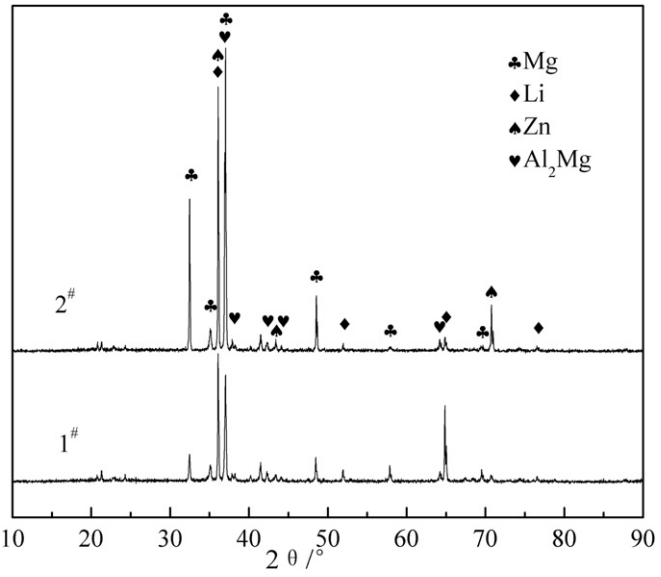

Fig. 1. XRD patterns of (1#) Mg–8Li–3Al–0.5Zn and (2#) Mg–8Li–3Al–1.0Zn alloys.

distortion caused by the different amount of Zn solid solution. This lattice distortion might influence the electrochemical behaviors of Mg–8Li–3Al–0.5Zn and Mg–8Li–3Al–1.0Zn alloys.

3.2. Potentiodynamic polarization

Fig. 2 shows the potentiodynamic polarization curves of Mg–8Li–3Al–0.5Zn and Mg–8Li–3Al–1.0Zn electrodes measured in 0.7 mol L^{-1} NaCl solution. The electrode was not soaked in the NaCl solution prior to the measurements. It can be observed from Fig. 2 that the corrosion potential of Mg–8Li–3Al–0.5Zn electrode is −1.58 V, which is slightly negative than that of Mg–8Li–3Al–1.0Zn electrode (−1.57 V). This implies that the fresh Mg–8Li–3Al–0.5Zn electrode has slightly higher electrochemical activity than that of the Mg–8Li–3Al–1.0Zn electrode when they are not soaked in 0.7 mol L^{-1} NaCl solution before measurements. The anodic current of Mg–8Li–3Al–0.5Zn electrode in the region closing to the corrosion potential is slightly higher than that of Mg–8Li–3Al–1.0Zn electrode, indicating that Mg–8Li–3Al–0.5Zn electrode is less corrosion resistive than that of Mg–8Li–3Al–1.0Zn electrode.

Fig. 3 shows the potentiodynamic polarization curves of Mg–8Li–3Al–0.5Zn and Mg–8Li–3Al–1.0Zn electrodes measured in 0.7 mol L^{-1} NaCl solution after they were soaked in 0.7 mol L^{-1} NaCl solution for 24 h. As can be seen that the corrosion potential of Mg–8Li–3Al–0.5Zn electrode is −1.52 V, which is also negative than that of Mg–8Li–3Al–1.0Zn electrode (−1.47 V), suggesting that after soaked in 0.7 mol L^{-1} NaCl solution for 24 h, the Mg–8Li–3Al–0.5Zn electrode still maintains the higher electrochemical activity than that of Mg–8Li–3Al–1.0Zn electrode.

Fig. 4a and b shows the SEM images of Mg–8Li–3Al–0.5Zn and Mg–8Li–3Al–1.0Zn electrodes, respectively. The images were taken after the electrodes were soaked in 0.7 mol L^{-1} NaCl solution for 24 h and then potentiodynamic polarized. Fig. 4a indicated that the oxidation product of Mg–8Li–3Al–0.5Zn electrode presents thick and large micro-blocks on the surface. Fig. 4b demonstrated that the surface of Mg–8Li–3Al–1.0Zn electrode shows fine and even crackles. This result means that Mg–8Li–3Al–1.0Zn is more corrosion resistive than Mg–8Li–3Al–0.5Zn alloy, which is

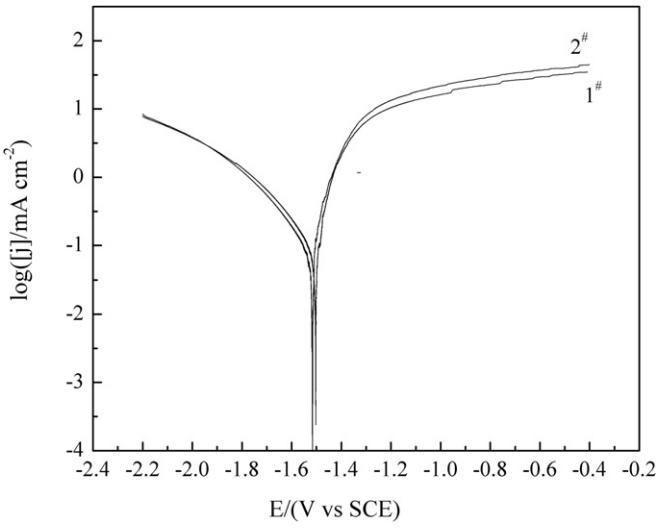

Fig. 2. Potentiodynamic polarization curves for (1#) Mg–8Li–3Al–0.5Zn and (2#) Mg–8Li–3Al–1.0Zn electrodes measured in 0.7 mol L^{-1} NaCl solution without soaking in 0.7 mol L^{-1} NaCl solution before measurements. Scan rate: 10 mV s^{-1}.

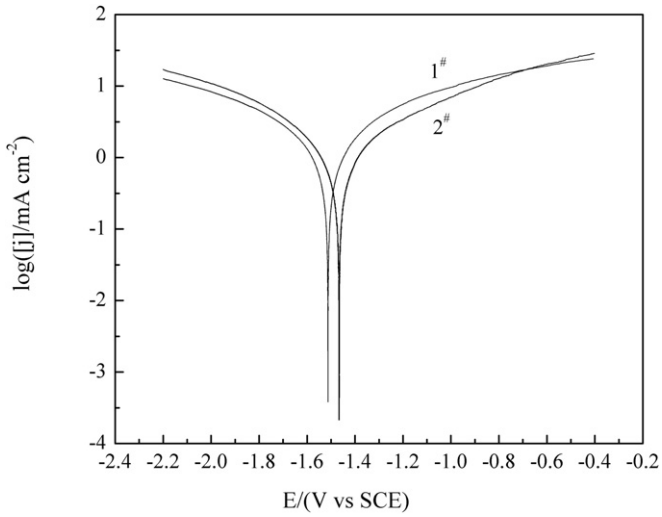

Fig. 3. Potentiodynamic polarization curves for (1#) Mg–8Li–3Al–0.5Zn and (2#) Mg–8Li–3Al–1.0Zn electrodes in 0.7 mol L^{-1} NaCl solution after soaking in 0.7 mol L^{-1} NaCl solution for 24 h.

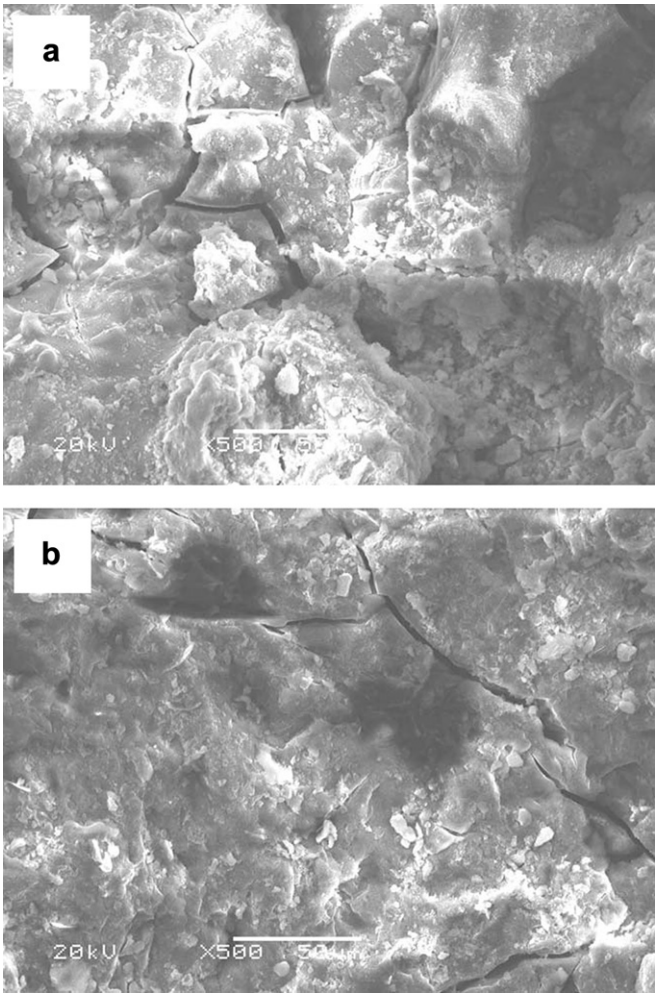

Fig. 4. SEM micrographs of (a) Mg–8Li–3Al–0.5Zn, (b) Mg–8Li–3Al–1.0Zn electrodes obtained after being soaked in 0.7 mol L^{-1} NaCl solution for 24 h and undergoes potentiodynamic polarization measurements.

consistent with the result obtained from potentiodynamic polarization measurements.

3.3. Potentiostatic oxidation

The current–time curves measured at −1.0 V in 0.7 mol L^{-1} NaCl solution for Mg–8Li–3Al–0.5Zn and Mg–8Li–3Al–1.0Zn electrodes are shown in Fig. 5. The current–time profiles are similar for the two samples. The anodic current increased rapidly in the early discharging stage and then reached to an approximately constant value. Mg–8Li–3Al–0.5Zn electrode displays a higher anodic current density than that of Mg–8Li–3Al–1.0Zn electrode, indicating that the Mg–8Li–3Al–0.5Zn electrode is more active than the Mg–8Li–3Al–1.0Zn electrode. By looking at the initial discharge period, it can be found that it took shorter time for the discharge current to reach to the steady value for Mg–8Li–3Al–1.0Zn electrode than that for Mg–8Li–3Al–0.5Zn electrode, which means that the Mg–8Li–3Al–1.0Zn electrode has shorter activation time and shorter voltage transition on switching between loads than Mg–8Li–3Al–1.0Zn electrode.

Fig. 6 displays the electrochemical impedance spectra of Mg–8Li–3Al–0.5Zn and Mg–8Li–3Al–1.0Zn electrodes at the open circuit potential in 0.7 mol L^{-1} NaCl solution. The single middle frequency capacitive arc is considered to be caused by charge transfer [21,22] and the diameter of the semicircle represents the polarization resistance R_p. The R_p of Mg–8Li–3Al–1.0Zn electrode (ca. 44.5 Ω cm^{-2}) is larger than that of Mg–8Li–3Al–0.5Zn electrode (ca. 32.5 Ω cm^{-2}). This indicates that the charge transfer activity of the Mg–8Li–3Al–0.5Zn electrode is higher than that of Mg–8Li–3Al–1.0Zn electrode and the corrosion resistance of Mg–8Li–3Al–1.0Zn electrode is bigger than that of Mg–8Li–3Al–0.5Zn electrode. Therefore, the content of Zn obviously affected the electrochemical activity and corrosion resistance of the alloys. These results are in good consistent with the results obtained from potentiodynamic polarization curves (Figs. 2 and 3) and current–time curves (Fig. 5).

Fig. 7a and b shows the SEM images of Mg–8Li–3Al–0.5Zn and Mg–8Li–3Al–1.0Zn electrodes after discharging at −1.0 V for 20 min in 0.7 mol L^{-1} NaCl solution. It can be observed that the surface of Mg–8Li–3Al–1.0Zn electrode shows fine and even

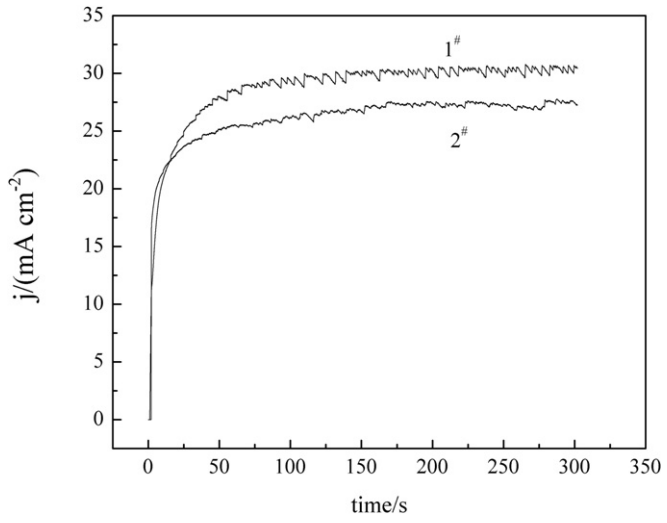

Fig. 5. Current–time curves for (1#) Mg–8Li–3Al–0.5Zn and (2#) Mg–8Li–3Al–1.0Zn electrodes recorded in 0.7 mol L^{-1} NaCl solution at a constant potential of −1.0 V for 5 min.

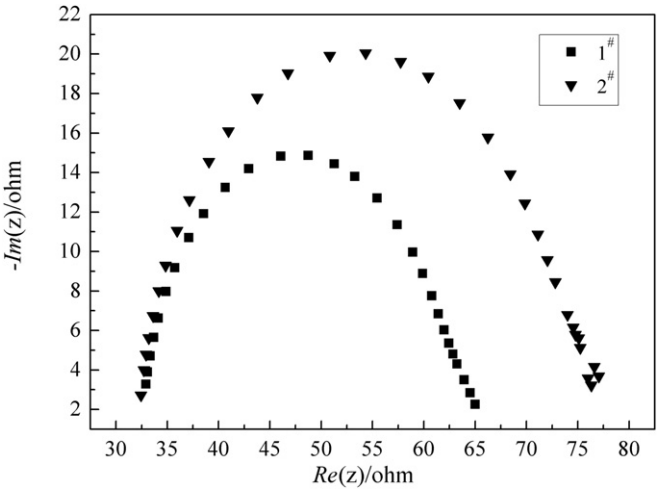

Fig. 6. The impedance spectra of (1#) Mg–8Li–3Al–0.5Zn and (2#) Mg–8Li–3Al–1.0Zn electrodes recorded in 0.7 mol L^{-1} NaCl solution.

crackles, but the Mg–8Li–3Al–0.5Zn electrode surface displays deeper and larger channels. Clearly, the morphologies of the oxidized surface of the two electrodes are different. The deeper and larger channels on the surface of Mg–8Li–3Al–0.5Zn electrode

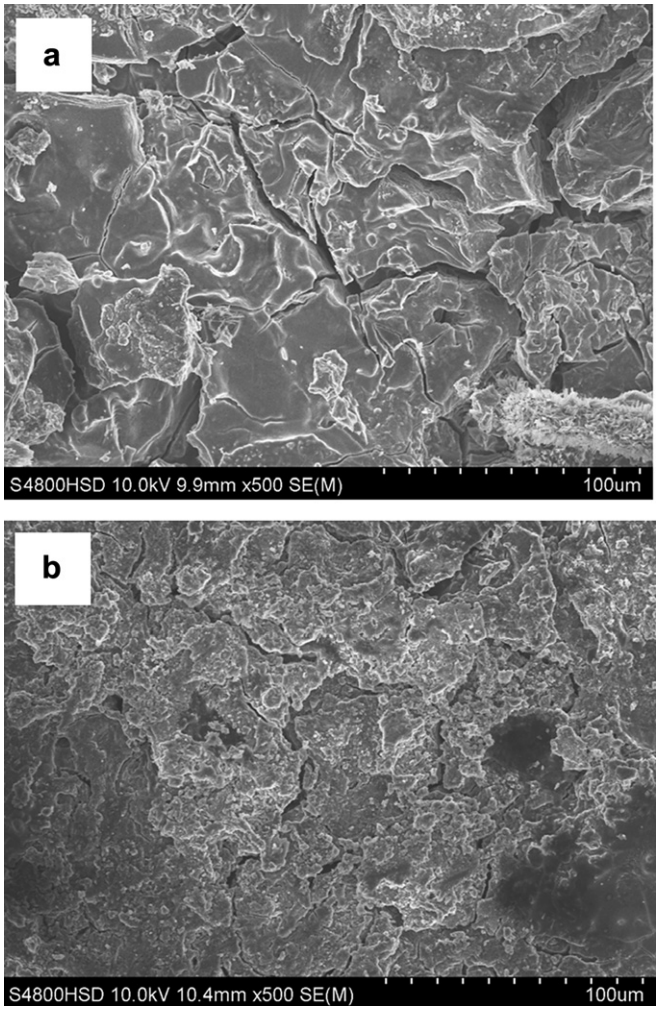

Fig. 7. SEM micrographs of (a) Mg–8Li–3Al–0.5Zn, (b) Mg–8Li–3Al–1.0Zn obtained after potentiostatic discharge at −1.0 V for 20 min in 0.7 mol L^{-1} NaCl solution.

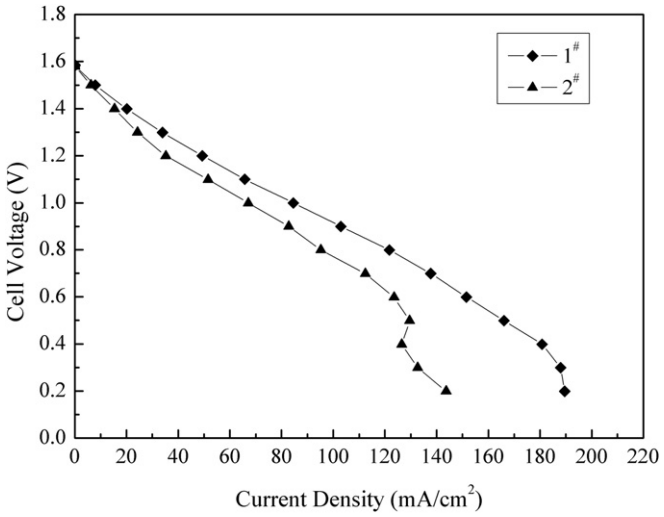

Fig. 8. The plots of the current density vs. cell voltage for the Mg–H_2O_2 semi fuel cell with (1#) Mg–8Li–3Al–0.5Zn and (2#) Mg–8Li–3Al–1.0Zn anodes at room temperature. Anolyte: 0.7 mol L^{-1} NaCl. Catholyte: 0.7 mol L^{-1} NaCl + 0.5 mol L^{-1} H_2O_2 + 0.1 mol L^{-1} H_2SO_4. Flow rate: 85 mL min^{-1}.

allow the electrolyte to penetrate through easily and also allow the oxidation products to come off more easily. Consequently, the Mg–8Li–3Al–0.5Zn electrode retains larger reaction surface area than the Mg–8Li–3Al–1.0Zn electrode during discharge, which might be responsible for the higher discharge current density of the Mg–8Li–3Al–0.5Zn electrode than the Mg–8Li–3Al–1.0Zn electrode.

3.4. Fuel cell performance

In order to evaluate the performance of Mg–8Li–3Al–0.5Zn and Mg–8Li–3Al–1.0Zn alloys as the anode of Mg–H_2O_2 semi fuel cells, the Mg–H_2O_2 semi fuel cells were assembled and their discharge performances were tested. Fig. 8 displays the plots of cell voltage versus current density. It can be seen that the voltage of the cell using Mg–8Li–3Al–0.5Zn anode is similar with Mg–8Li–3Al–1.0Zn anode at low current density. With the increase of current density, the Mg–8Li–3Al–0.5Zn anode exhibited better performance than that of Mg–8Li–3Al–1.0Zn anode, especially at current density higher than 30 mA cm^{-2} Fig. 9 shows the plots of the power density versus current density. The peak power density of the semi-fuel cell with Mg–8Li–3Al–0.5Zn anode reached 100 mW cm^{-2}, which is higher than that of Mg–8Li–3Al–1.0Zn anode (80 mW cm^{-2}). Accordingly, the Mg–8Li–3Al–0.5Zn alloy is a better anode material for the semi-fuel cell than the Mg–8Li–3Al–1.0Zn alloy. It has been reported that the peak power density for the semi-fuel cell using pure Mg as the anode material is 83.36 mW cm^{-2} [20], which is lower than that using Mg–8Li–3Al–0.5Zn as the anode material reported in this work (100 mW cm^{-2}). So, the performance of Mg–8Li–3Al–0.5Zn alloy is better that that of Mg.

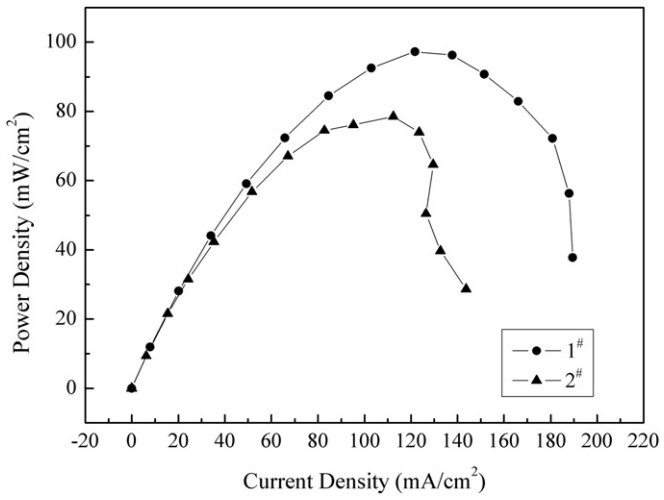

Fig. 9. The plots of the current density vs. power density for the Mg–H_2O_2 semi fuel cell with (1#) Mg–8Li–3Al–0.5Zn and (2#) Mg–8Li–3Al–1.0Zn anodes at room temperature. Anolyte: 0.7 mol L^{-1} NaCl. Catholyte: 0.7 mol L^{-1} NaCl + 0.5 mol L^{-1} H_2O_2 + 0.1 mol L^{-1} H_2SO_4. Flow rate: 85 mL min^{-1}.

4. Conclusions

The electrochemical oxidation behaviors of Mg–8Li–3Al–0.5Zn and Mg–8Li–3Al–1.0Zn electrodes in 0.7 mol L^{-1} NaCl solution and their performances as the anode of Mg–H_2O_2 semi fuel cells were investigated. The Mg–8Li–3Al–0.5Zn electrode shows higher discharge activity and lower corrosion resistance than the Mg–8Li–3Al–1.0Zn electrode in 0.7 mol L^{-1} NaCl solution. The peak power density of Mg–H_2O_2 semi fuel cell with the Mg–8Li–3Al–0.5Zn anode (100 mW cm^{-2}) is higher than that with Mg–8Li–3Al–1.0Zn anode (80 mW cm^{-2}). The content of Zn in alloys obviously affected the performance of the alloys and the Zn content of 0.5% is better than 1.0%.

Acknowledgments

This work was financially supported by the Natural Science Foundation of Heilongjiang Province of China (B201201), National Natural Science Foundation of China (No. 21203040), the Fundamental Research Funds for the Central Universities (HEUCF201210010) and the Specialized Research Fund for the Doctoral Program of Higher Education (20102304110001). The authors are grateful for Dr. Milin Zhang and Ruizhi Wu for assistance in alloy preparation.

References

[1] O. Hasvold, N.J. Storkersen, S. Forseth, T. Lian, J. Power Sources 162 (2006) 935.
[2] M.G. Medeiros, R.R. Bessette, C.M. Deschenes, C.J. Patrissi, L.G. Carreiro, S.P. Tucker, D.W. Atwater, J. Power Sources 136 (2004) 226–231.
[3] R.R. Bessette, M.G. Medeiros, C.J. Patrissi, C.M. Deschenes, C.N. LaFratta, J. Power Sources 96 (2001) 240–244.
[4] R.R. Bessette, J.M. Cichon, D.W. Dischert, E.G. Dow, J. Power Sources 80 (1999) 248–253.
[5] W. Yang, S. Yang, W. Sun, G. Sun, Q. Xin, J. Power Sources 160 (2006) 1420.
[6] W. Yang, S. Yang, W. Sun, G. Sun, Q. Xin, Electrochim. Acta 52 (2006) 9.
[7] D.J. Brodrecht, J.J. Rusek, Appl. Energy 74 (2003) 113–124.
[8] M.G. Medeiros, C.G. Zoski, J. Phys. Chem. B 102 (1998) 9908–9914.
[9] S. Ono, K. Asami, T. Osaka, N. Masuko, J. Electrochem. Soc. 143 (1996) 106–109.
[10] D.L. Song, X.Y. Jing, J. Wang, J. Corros. Sci. 53 (2011) 3651–3656.
[11] W.Q. Yang, S.H. Yang, W. Sun, J. Sci. Direct 52 (2006) 9–14.
[12] M.G. Medeiros, R.R. Bessette, C.M. Deschenes, D.W. Atwater, J. Power Sources 96 (2001) 236–239.
[13] M.G. Medeiros, E.G. Dow, J. Power Sources 80 (1999) 78–82.
[14] A. Sivashanmugam, T.P. kumar, N.G. Renganathan, S. Gopukumarl, J. Appl. Electrochem. 34 (2004) 1135–1139.
[15] C.Z. Shu, E.D. Wang, L.H. Jiang, J. Power Sources 208 (2012) 159–164.
[16] Y.B. Ma, N. Li, D.Y. Li, J. Power Sources 196 (2011) 2346–2350.
[17] D.X. Cao, X. Cao, G.L. Wang, L. Wu, Z.S. Li, J. Solid State Electrochem 14 (2010) 851–855.
[18] D.X. Cao, L. Wu, Y. Sun, G.L. Wang, Y.Z. Lv, J. Power Sources 177 (2008) 624–630.
[19] D.X. Cao, L. Wu, G.L. Wang, Y.Z. Lv, J. Power Sources 183 (2008) 799–804.
[20] Y.Z. Lv, Y. Xu, D.X. Cao, J. Power Sources 196 (2011) 8809–8814.
[21] M. Anik, G. Celikten, J. Corros. Sci. 49 (2007) 1878–1894.
[22] G. Song, A. Atrens, X. Wu, et al., J. Corros. Sci. 40 (1998) 1769–1791.